Journal of Materials Chemistry A

PAPER

View Article Online
View Journal | View Issue

Cite this: J. Mater. Chem. A, 2014, 2, 9514

Responsive Au@polymer hybrid microgels for the simultaneous modulation and monitoring of Au-catalyzed chemical reaction†

Chuanfu Xiao, Qingshi Wu, Aiping Chang, Yahui Peng, Wenting Xu and Weitai Wu*

Received 23rd January 2014
Accepted 14th March 2014

DOI: 10.1039/c4ta00409d

www.rsc.org/MaterialsA

The simultaneous modulation and monitoring of catalysis is possible when using metal@polymer hybrid microgels by rational design. Such hybrid microgels are made of Au nanoparticles covered with a temperature and pH dual-responsive copolymer gel shell of poly(*N*-isopropylacrylamide-*co*-allylamine). The Au nanoparticle cores can act as catalysts in a model electron-transfer reaction between hexacyanoferrate(III) and borohydride ions. The introduction of a smart polymer gel shell onto the Au nanoparticles can not only allow modulation of the catalysis of the Au nanoparticle cores through varying the solution temperature, but also allow label-free *in situ* localized surface plasmon resonance (LSPR) monitoring of the kinetics and thermodynamics of the catalyzed chemical reaction. Unlike conventional spectroscopic methods that only reflect the overall information occurring in the reaction system, the label-free *in situ* LSPR monitoring gives local information occurring on the catalytic surface and therefore has the potential to advance our understanding of the catalyzed chemical reaction.

Introduction

Responsive hybrid materials, comprising inorganic nanoparticles covered with smart polymers, have been receiving a great deal of attention.[1–13] While inorganic nanoparticles exhibit size-, shape-, and interdistance-dependent catalytic and optical properties,[14–21] smart polymers can undergo a volume phase transition in response to external stimuli, such as temperature, pH, or a specific molecule,[22–25] to modify the physicochemical environment of the components embedded inside. Thus, hybrid materials with inorganic nanoparticles embedded in smart polymers, combining the unique properties from both inorganic nanoparticles and smart polymers, offer possibilities for external manipulation of the functionalities of inorganic nanoparticles, providing a functional basis for smart systems for prospective applications in many fields.

Materials with stimuli-responsive catalytic properties are becoming more and more important for application in catalysis, as their catalytic activity may be tuned by applying external stimuli.[4–12,26,27] Immobilization of noble metal nanoparticles in smart polymer microgels is one way to make materials with stimuli-responsive catalytic properties. Ballauff and co-workers were the first to develop such materials, *via in situ* synthesis of metallic nanoparticles in temperature-responsive polystyrene-poly(*N*-isopropylacrylamide) (PSt-PNIPAM) microgels.[7,8] Metal@polymer hybrid microgels have the advantage that the metal nanoparticles are embedded in a polymer network that prevents aggregation with other nanoparticles, and the catalytic activity of the metal nanoparticles can be tuned by the swelling and shrinking of the polymer gels. Those hybrid microgels have been proven efficient catalysts for several chemical reactions.[4–6] Liz-Marzán and co-workers developed Au@PNIPAM core–shell hybrid microgels, *via* growth of polymer gels on Au nanoparticles.[9] They found that the temperature-responsive PNIPAM gel shell with limited cross-linking allowed for particularly efficient control of the catalysis of the embedded Au nanoparticles.[10,11] Recently, we reported a one-pot synthetic approach to pH-responsive Au@polyvinylpyrrolidone core–shell hybrid microgels, which also has the potential to modulate Au-catalyzed chemical reactions.[12]

In this work, we aim to demonstrate the concept that metal@polymer hybrid microgels under rational design can not only allow modulation of the catalysis of embedded noble metal nanoparticles, but also allow label-free *in situ* localized surface plasmon resonance (LSPR) monitoring of the catalyzed chemical reaction. It should be noted that in a reaction system comprising metal@polymer hybrid microgels dispersed in liquid media, the label-free *in situ* monitoring of a metal-catalyzed chemical reaction remains a challenge for two main reasons: (i) chemical transformations are confined to the metal surface, and (ii) trace or unstable reaction products on the catalytic surface are difficult to separate and purify. LSPR effects in noble metal nanoparticles can be

State Key Laboratory for Physical Chemistry of Solid Surfaces, and Department of Chemistry, College of Chemistry and Chemical Engineering, Xiamen University, Xiamen 361005, Fujian, China. E-mail: wuwtxmu@xmu.edu.cn; Fax: +86-592-2185862; Tel: +86-592-2185862

† Electronic supplementary information (ESI) available: Fig. S1, Fig. S2, and Fig. S3. See DOI: 10.1039/c4ta00409d

observed in a UV-vis spectrum.[16,17] To date, *in situ* LSPR monitoring of a local microenvironment has been demonstrated on a number of metal@polymer hybrid microgels.[1–3,9,12] The stimuli-responsive volume phase transitions of smart polymer gels can lead to changes in the immediate physicochemical microenvironment (*e.g.*, the local refractive index) of noble metal nanoparticles, hence, resulting in an alternation of the LSPR.[28] In this respect, *in situ* LSPR sensing should also offer exceptional possibilities, as in other cases of plasmon-assisted sensing of catalytic reactions.[29–33] Unlike the conventional spectroscopic methods that only reflect the overall information occurring in the reaction system, *in situ* LSPR monitoring may give local information occurring on the catalytic surface and therefore has the potential to advance our understanding of the catalyzed chemical reaction. However, to the best of our knowledge, no report of any metal@polymer hybrid microgels for the simultaneous modulation and monitoring of a catalyzed chemical reaction has appeared in the literature.

The metal@polymer hybrid microgel, depicted in Scheme 1, was designed to consist of Au nanoparticles covered with a temperature and pH dual-responsive copolymer gel shell of poly(*N*-isopropylacrylamide-*co*-allylamine)(p(NIPAM-Am)), and was denoted Au@p(NIPAM-Am). To demonstrate the performance of the hybrid microgels, we selected the electron transfer reaction between hexacyanoferrate(III) and borohydride ions in water as a model, a standard redox reaction which is efficiently catalyzed on the Au nanoparticle surface in comparison with catalyst-free conditions.[34,35] An advantage with this reaction as a model is that it can be monitored by using conventional spectroscopic methods through following the changes in the hexacyanoferrate(III) absorption,[34,35] and thus the reaction kinetics and thermodynamics measured by *in situ* LSPR monitoring can be compared. We show that the kinetics measured by both methods revealed nearly the same trend at the investigated temperatures, whereas a difference between the thermodynamics measured by the two methods was observed.

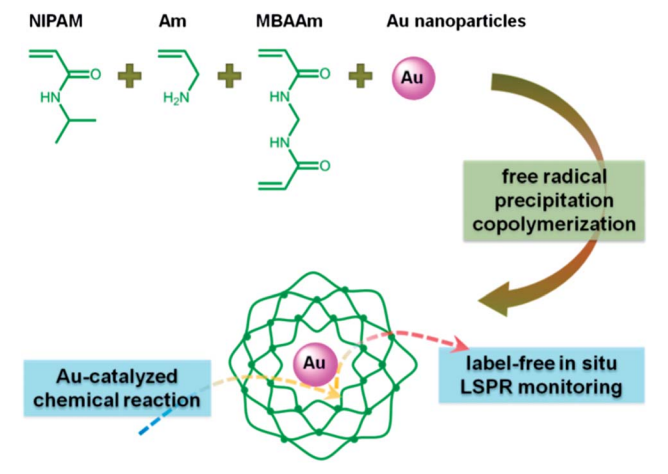

Scheme 1 Schematic illustration of a responsive Au@polymer hybrid microgel, comprising Au nanoparticles covered with a temperature and pH dual-responsive copolymer gel shell of poly(*N*-isopropylacrylamide-*co*-allylamine)(p(NIPAM-Am)), for the simultaneous modulation and monitoring of a Au-catalyzed chemical reaction.

Experimental section

Materials and reagents

Hydrogen tetrachloroaurate(III) hydrate ($HAuCl_4 \cdot 3H_2O$), sodium borohydride ($NaBH_4$), L-(+)-ascorbic acid (L-AA), trihydrate citrate dehydrate (Tc), polyvinylpyrrolidone (PVP, $M_w \approx 58\,000$), potassium iodide (KI), sodium dodecyl sulfate (SDS), styrene (St), and *N*,*N*,*N*′,*N*′-tetramethylethylenediamine (TEMED) were purchased from Alfa Aesa. NIPAM, *N*,*N*′-methylenebisacrylamide (MBAAm), divinylbenzene (DVB), 2,2′-azobis(2-methylpropionamidine) dihydrochloride (AAPH), and ammonium persulfate (APS) were purchased from Aldrich. Potassium hexacyanoferrate(III) was purchased from Sinopharm Chemical Reagent Co. Ltd. Allylamine (Am) was purchased from Best Reagent Co. Ltd. NIPAM was recrystallized from a hexane–acetone (a 1 : 1 volume ratio) mixture and dried in a vacuum. St and DVB were purified with neutral Al_2O_3. All other chemicals were used as received without further purification. The water used in all experiments was of Millipore Milli-Q grade.

Synthesis of Au nanoparticles

$HAuCl_4$ (1.0 mL, 5.0 mM), Tc (1.0 mL, 5.0 mM) and H_2O (18.0 mL) were mixed in a flask. After vigorously stirring for 2 min, fresh $NaBH_4$ solution (0.6 mL, 0.1 M) was quickly added. The color of the mixture immediately changed to yellowish red. The mixture was further stirred for 4 h and then collected as the seed solution for subsequent seed growth. In the next step, $HAuCl_4$ (0.6 mL, 0.25 M), PVP (5.0 mL, 5.0 wt %), L-AA (2.5 mL, 0.1 M), KI (2.0 mL, 0.2 M) and H_2O (20.0 mL) were mixed in a flask and gently stirred for 10 min, then the as-prepared seed solution (375.0 μL) was added. The reaction was continued for another 10 min. The obtained reddish brown Au nanoparticles were collected, and PVP and other unreacted compounds were removed by repeated centrifugation (8000 rpm, 20 min, 25 °C) and washing with water, and redispersed in water (1000.0 mL).

Synthesis of Au@p(NIPAM-Am) hybrid microgels

Am (124.0 μL) was dropwise added into the as-prepared Au nanoparticles solution (50.0 mL) in a round-bottom flask. After stirring for 1 h, SDS (3.0×10^{-2} g) was added. This mixture was further stirred overnight. After addition of NIPAM (3.8×10^{-1} g) and MBAAm (5.0×10^{-2} g), the mixture was purged with N_2 for 30 min and then heated to 50 °C. The polymerization was initiated by adding APS (0.7 mL, 1.2×10^{-1} M)/TEMED (0.7 mL, 2.4×10^{-1} M). The red solution became turbid within 10 min and the reaction was allowed to proceed for a total of 3 h. The product was purified by centrifugation (8000 rpm, 30 min, 25 °C) and redispersed in water (50.0 mL) six times, followed by 3 days of dialysis against very frequently changed water.

Synthesis of Au@p(NIPAM) hybrid microgels

Au@p(NIPAM), which served as a control, was synthesized by a two-step method first involving St then followed by NIPAM,

because the coating of the Au nanoparticle core with the gel layer of St should favor subsequent covering with a gel layer of NIPAM.[9] The as-prepared Au nanoparticles (80.0 mL) and SDS (3.0×10^{-2} g) were mixed and stirred for 30 min, and St (80.0 μL) and DVB (16.0 μL) were added. After being purged with a N_2 flow for 30 min, the solution was heated to 70 °C. The polymerization was initiated by adding AAPH (0.2 mL, 0.1 M). The polymerization was allowed to proceed for 2 h. The product was collected by centrifugation (8000 rpm, 30 min, 25 °C), and then redispersed in water (80.0 mL). This dispersion (50.0 mL) and SDS (3.0×10^{-2} g) were mixed and stirred for 10 h at room temperature, followed by adding NIPAM (1.7×10^{-1} g) and MBAAm (2.3×10^{-2} g). After being purged with a N_2 flow for 30 min, the mixture was heated to 70 °C and initiated by adding APS (0.4 mL, 1.2×10^{-1} M). The reddish dispersion became turbid within 10 min. The reaction was continued for 3 h. The product was purified by centrifugation (8000 rpm, 30 min, 25 °C) and redispersed in water three times, followed by 3 days of dialysis against very frequently changed water at room temperature.

Dynamic laser light scattering (DLS) studies

DLS was performed on a 90Plus multi angle particle sizing analyzer equipped with a BI-9000AT digital autocorrelator (Brookhaven Instruments, Inc.) to measure the average hydrodynamic diameter ($\langle D_h \rangle$) and the size distribution. A He–Ne laser (35 mW, 659 nm) was used as the light source. All hybrid microgel dispersions were passed through Millipore Millex-HV filters with a pore size of 0.80 μm to remove dust before DLS measurements. In DLS, the Laplace inversion (here the CONTIN method was used) of each measured intensity–intensity time correlation function in a dilute dispersion can lead to a line-width distribution $G(\Gamma)$. For a purely diffusive relaxation, Γ is related to the translational diffusion coefficient D by $(\Gamma/q^2)_{C\to 0, q\to 0} = D$, so that $G(\Gamma)$ can be converted to a translational diffusion coefficient distribution and $\langle D_h \rangle$ distribution by using the Stokes–Einstein equation, $\langle D_h \rangle = (k_B T/3\pi\eta)/D$, where k_B, T, and η are the Boltzmann constant, the absolute temperature, and the solvent viscosity, respectively.[36] All DLS measurements were made at a scattering angle of $\theta = 90°$.

pH-responsive LSPR of the hybrid microgels

To study the LSPR response, hybrid microgels (1.5 mL) of different pH values were stirred in a quartz cuvette, which was placed inside a UV-vis spectrophotometer equipped with a temperature controller (±0.1 °C) (Agilent model 8453 UV-vis spectrophotometer). After incubation for 20 min at a designed temperature, the UV-vis spectrum was recorded for further analysis.

The pH resolution (δpH) was evaluated by:[37]

$$\delta\mathrm{pH} = \left(\frac{\partial x}{\partial y}\right)\delta I_{\mathrm{pH}} \quad (1)$$

where $\partial x/\partial y$ and δI_{pH} represent the inverse of the slope in the LSPR intensity *versus* the pH value diagram and the standard deviation of the LSPR intensity, respectively. The $\partial x/\partial y$ was obtained by differentiating the polynomial fitting of the plot of the LSPR intensity *versus* the pH value, and δI_{pH} was calculated with the following eqn (2) as the averaged difference between I_{pH} and the LSPR intensity experimentally acquired:

$$\delta I_{\mathrm{pH}} = \frac{\sum_{i=1}^{n} |I_{\mathrm{pH}} - I_{\mathrm{pH},i}|}{n} \quad (2)$$

where n and $I_{pH,i}$ imply the repeat time (here $n = 5$) and the LSPR intensity of each measurement at a pH value, respectively.

Experiments on the model Au-catalyzed chemical reaction

The model chemical reaction was conducted in a quartz cuvette, which was placed inside a UV-vis spectrophotometer equipped with a temperature controller (±0.1 °C). Typically, the hybrid microgels (1.5 mL) and $NaBH_4$ (1.0 mL, 250.0 mM) were stirred together in the quartz cuvette at a designated temperature for 5 min. The initial pH values of all reaction mixtures were set to 10.50. $K_3Fe(CN)_6$ (50.0 μL, 0.1 M) was then added into the mixture, which was stirred until the yellow reddish solution became red. During the course of the reaction, the progress was *in situ* monitored by measuring the UV-vis absorption spectra of the mixture. Experiments were reproducible to within 5%. The data was then analysed by using the $Fe(CN)_6^{3-}$ absorption or the LSPR band.

Other characterization

Fourier transform infrared (FTIR) spectra were recorded on a Thermo Electron Corporation Nicolet 380 Fourier transform infrared spectrometer. Transmission electron microscopy (TEM) images were taken on a JEOL JEM-1400 transmission electron microscope at an acceleration voltage of 100 kV. The pH values were obtained on a METTLER TOLEDO SevenEasy pH meter (±0.0005). The contents of Au in the hybrid microgels were determined by using a Dionex ICS-1500 ion chromatography system.

Result and Discussion

Synthesis of Au@p(NIPAM-Am) hybrid microgels

The size distribution was characterized by using *in situ* DLS at 25.0 °C. The Au nanoparticles and Au@p(NIPAM-Am) hybrid microgels were compared as shown in Fig. 1a. Both the Au nanoparticles and the hybrid microgels were narrowly distributed with a polydispersity index $\mu_2/\langle\Gamma\rangle^2 \leq 0.005$. The hybrid microgels had a larger $\langle D_h \rangle$ of 260 nm than the Au nanoparticles ($\langle D_h \rangle = 32$ nm). The increased particle size and narrow distribution indicate that the polymer gels had been added onto the Au nanoparticles, and the formation of new homo-polymer particles during the synthesis of the hybrid microgels was negligible. In the FTIR spectra of the purified hybrid microgels (Fig. 1b), the characteristic bands of the carbonyl stretching vibration (amide I) at 1660 cm^{-1} and N–H bending vibration (amide II) at 1548 cm^{-1}, as well as the two typical bands of C–H vibrations of $-CH(CH_3)_2$ at 1384 cm^{-1} and 1368 cm^{-1}, of the NIPAM units were recorded. The characteristic NH_2 symmetric

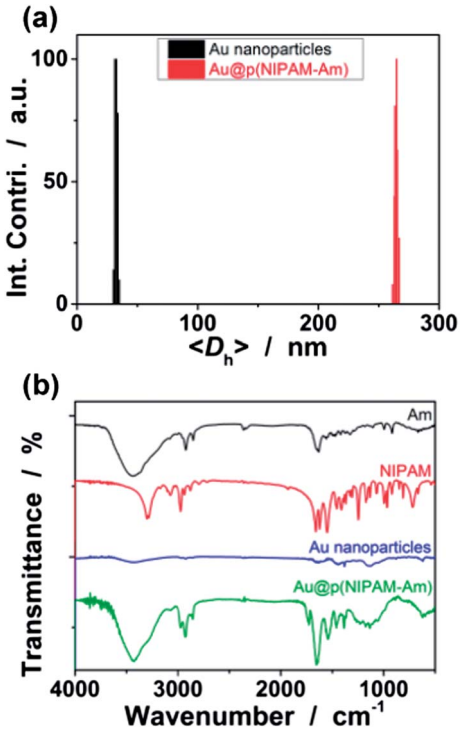

Fig. 1 (a) DLS size distribution of Au nanoparticles and Au@p(NIPAM-Am) hybrid microgels, measured at 25.0 °C. (b) FTIR spectra.

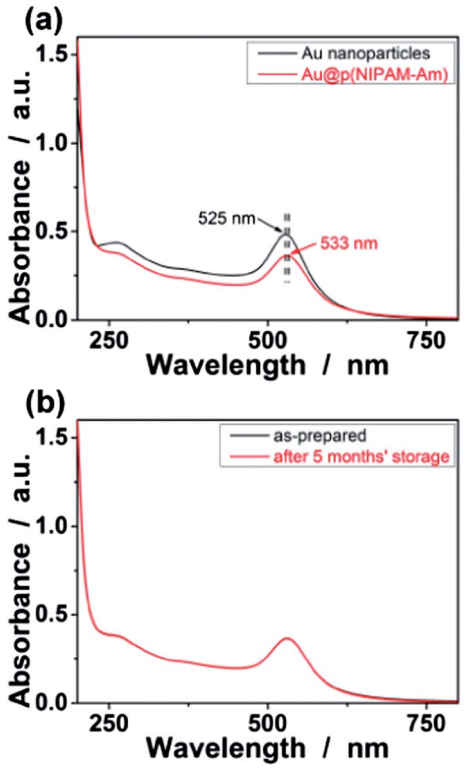

Fig. 3 (a) UV-vis spectrum of Au@p(NIPAM-Am) hybrid microgels and Au nanoparticles. (b) UV-vis spectra of Au@p(NIPAM-Am) hybrid microgels before and after 5 months' storage at room temperature.

and asymmetric absorption bands of the Am units appeared at 1541 cm^{-1} and 1367 cm^{-1}, respectively. Given the monomer reactivity ratios $r_{12} = 1.04$ and $r_{21} = 0.95$ for NIPAM (r_1) and the acrylamide (r_2) monomer pairs,[38] together with $r'_{12} = 13.35$ and $r'_{21} = 0.08$ for acrylamide (r'_1) and the Am (r'_2) monomer pairs,[39] the p(NIPAM-Am) gel may possess random functional NIPAM and Am units through the polymer network chains.

The TEM image (Fig. 2a) of the Au@p(NIPAM-Am) hybrid microgels indicates a core–shell morphology with a black dot embedded in a gray matrix (*ca.* 200 nm thick). The size of the black dot is consistent with that of a Au nanoparticle (36 ± 5 nm; Fig. 2b), revealing a uniform distribution without significant aggregation of the Au nanoparticles embedded inside the polymer gels. The successful coating of the polymer gel shell also manifests as a red-shift of *ca.* 8 nm (35.4 meV; Fig. 3a) on the peak plasmon absorption of the hybrid microgels (centered at 533 nm), in comparison with that of the Au nanoparticles (centered at 525 nm). This red-shift in the peak plasmon absorption is related to a change in local dielectric constant around the Au nanoparticles as a result of their encapsulation in the polymer gels.[40–42] The hybrid microgels are reproducible from batch to batch, with a high yield of ≥86%. Moreover, the hybrid microgels show good stability. No sediment was observed after at least 6 months' storage at room temperature. Only a marginal change in the UV-vis spectrum was observed (Fig. 3b), implying that the size and shape of the Au nanoparticle cores remained nearly unchanged and the aggregate/leaching of the Au nanoparticle cores was negligible.

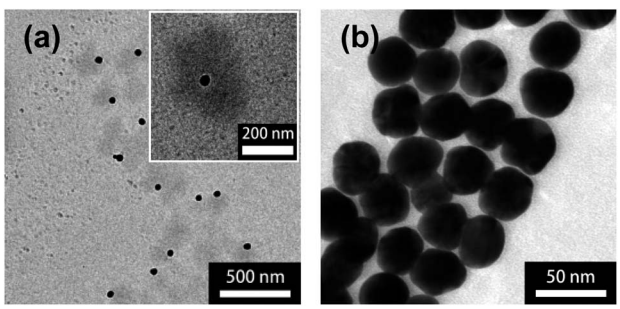

Fig. 2 TEM image of (a) Au@p(NIPAM-Am) hybrid microgels and (b) Au nanoparticles.

Stimuli-responsive volume phase transition of Au@p(NIPAM-Am) hybrid microgels

High porosity of the polymer gel shell is crucial for application of the Au@p(NIPAM-Am) hybrid microgels in catalysis. The polymer gel shell covering the Au nanoparticle cores should be so permeable to both reactants and products that mass-transfer limitations can be avoided to maximize the reaction rates. Since the porosity of the stimuli-responsive polymer gels can be characterized by their volume phase transitions in response to an environmental condition change,[22–25] we then examined the effect of the solution temperature and the solution pH value, respectively, on the Au@p(NIPAM-Am) hybrid microgels by

using *in situ* DLS, which is a powerful tool to study volume phase transitions of polymer gel particles in solution.

Fig. 4a shows the temperature-responsive volume phase transition of the Au@p(NIPAM-Am) hybrid microgels at a solution pH value of 10.50 (the same solution pH value to that used for the catalytic experiments discussed below), in terms of the change in $\langle D_h \rangle$ measured at a scattering angle of $\theta = 90°$. It is clear that the $\langle D_h \rangle$ of the hybrid microgels significantly reduced at the elevated temperatures within our experimental temperature window of 15.0–55.0 °C. The broad volume phase transition region of the hybrid microgels could be attributed to crosslinking heterogeneity.[22] Fig. 4b shows the $\langle D_h \rangle$ of the hybrid microgels as a function of the solution pH value, as measured at a solution temperature of 25.0 °C (the same solution temperature to that used for the catalytic experiments discussed below) and a scattering angle of $\theta = 90°$. As expected, the Am units ($pK_a \approx 9.70$) on the polymer chains of the polymer gel shell exhibit well-defined pH-responsive volume phase transitions. When the solution pH value decreased from 11.10 to 5.90, the Am units were gradually deprotonated. The Coulombic repulsion among the ionized amine groups increased the osmotic pressure,[23] resulting in a gradual increase in the $\langle D_h \rangle$ until all Am groups were deprotonated at pH < 7.00, where the hybrid microgels reached a maximum swelling. Overall, the stimuli-responsive swelling ratios, $\langle D_h \rangle_{T=15°C,pH=10.50}/\langle D_h \rangle_{T=55°C,pH=10.50}$ and $\langle D_h \rangle_{T=25°C,pH=5.90}/\langle D_h \rangle_{T=25°C,pH=11.10}$, were determined to be 2.1 and 1.1, respectively, indicating the desired high sensitivity of the hybrid microgels to solution temperature, and an appropriate but not too high sensitivity to the solution pH value. The stimuli-responsive volume phase transitions of the Au@p(NIPAM-Am) hybrid microgels are fully reversible. This was demonstrated by the perfect match of the heating/cooling curves (Fig. 4a) and pH increasing/decreasing curves (Fig. 4b), respectively, as well as the repeatable size distribution during heating/cooling (Fig. 4c) and pH increasing/decreasing cycles (Fig. 4d). In contrast, the $\langle D_h \rangle$ of the free Au nanoparticles stayed nearly constant at approximately 32 nm in our experimental temperature (15.0–55.0 °C) and pH (5.90–11.10) windows, reflecting their good stability in the tested varied environments. Taken together, these results confirm the highly porous nature of the polymer gel shell of the hybrid microgels.

pH-responsive LSPR of Au@p(NIPAM-Am) hybrid microgels

Fig. 5a (also see Fig. S1 in ESI†) shows the pH-dependent UV-vis spectra, which were recorded on the aqueous dispersions of the Au@p(NIPAM-Am) hybrid microgels under a solution pH value between 7.53 (swollen state) and 10.55 (collapsed state) at 25.0 °C. Both a remarkable increase in the LSPR intensity (I_{pH}) and a slightly red shift in the LSPR position (*ca.* 1–3 nm) were observed with the increase in pH value. This is likely to be due to an increase in the refractive index of the polymer gel shell during its collapse, which results in an increase in the Rayleigh scattering because of a larger refractive index contrast with the solvent, as well as an increase in the local refractive index around the Au nanoparticle cores, which leads to an enhancement of the LSPR band, as previously reported and predicted by Mie theory.[9,28] The effect of the variation in the pH value on the LSPR is summarized in Fig. 5b, which gives the pH-responsive LSPR in a more orthogonal fashion. The pH resolution (δpH) was determined to be approximately 0.08–0.15 units over the pH range of 7.53–10.55 (Fig. 5c), indicating a high sensitivity for pH sensing. Due to the good stability and the fully reversible volume phase transitions of the hybrid microgels, the LSPR response is completely reversible (Fig. 5d).

Because the model chemical reaction used below involved changes in the concentration of salts, the pH-responsive LSPR was required to be free from significant interferences from those constituents. To this end, the Au@p(NIPAM-Am) hybrid

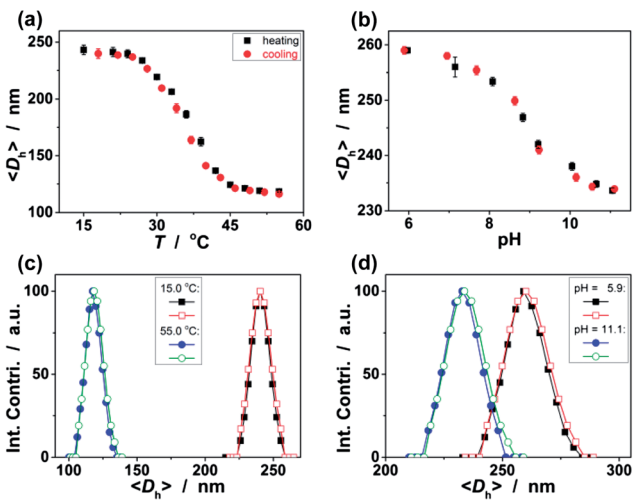

Fig. 4 (a) Temperature-dependent (pH = 10.50) and (b) pH-dependent (25.0 °C) $\langle D_h \rangle$ of Au@p(NIPAM-Am) hybrid microgels. (c and d) DLS size distribution of the hybrid microgels before (closed symbols) and after (open symbols) nine cycles of (c) heating/cooling and (d) pH increasing/decreasing, respectively.

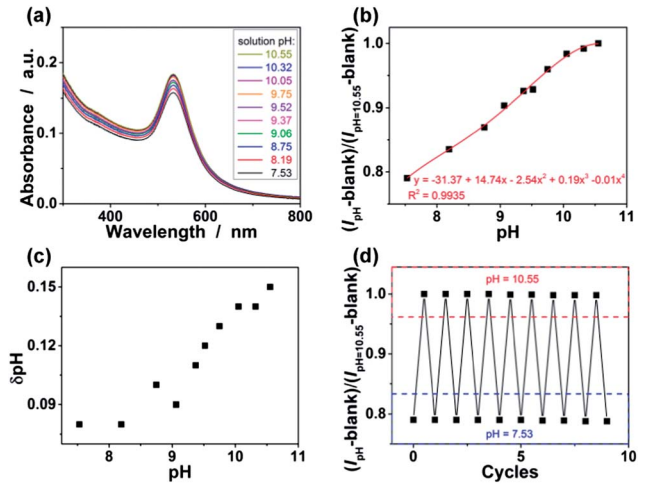

Fig. 5 (a) pH-dependent UV-vis spectra of Au@p(NIPAM-Am) hybrid microgels. (b) A plot showing the relationship between the LSPR intensity and the pH value. (c) pH resolution. (d) LSPR response cycles upon repeated pH increasing/decreasing.

microgels were first subjected to NaCl, as a salt source. When the NaCl concentration increased from 0 to 1.0 mM, an almost identical LSPR response to the pH variation was obtained with a relative error of less than ±1.3% (*i.e.*, within ±0.14 unit) over the range 7.53–10.55, demonstrating a minimal impact of the salt on the pH-responsive LSPR of the hybrid microgels. The interferences can be further eliminated when the enhanced LSPR intensity is expressed as a ratio of (I_{pH}–blank)/($I_{pH=10.55}$–blank) to evaluate the LSPR response. Similarly, the pH-responsive LSPR was independent of 0.1 mM borohydride, borate, hexacyanoferrate(II), or hexacyanoferrate(III) ions (with a relative error generally less than ±0.26%, *i.e.*, within ±0.03 units). Therefore, a high selectivity for pH sensing should be achieved by the Au@p(NIPAM-Am) hybrid microgels in the reaction system.

Modulating the catalytic activity of Au@p(NIPAM-Am) hybrid microgels

We then examined the catalytic activity of the Au@p(NIPAM-Am) hybrid microgels, with regard to the reduction of hexacyanoferrate(III) ($Fe(CN)_6^{3-}$) by borohydride (BH_4^-) ions in water, which has been proposed as a model reaction to evaluate the catalytic activity of Au nanoparticles.[10,34,35] The redox reaction can be written as[43]

$$BH_4^- + 8Fe(CN)_6^{3-} + 3H_2O \rightarrow H_2BO_3^- + 8Fe(CN)_6^{4-} + 8H^+ \quad (3)$$

In the presence of Au nanoparticles, the reaction proceeds through a two-step process. In the first step, BH_4^- ions inject electrons onto the Au nanoparticles, which act as a reservoir and become cathodically polarized, whereas in the second and slower step, $Fe(CN)_6^{3-}$ ions diffuse toward the Au nanoparticle surface and are reduced by the excess surface electrons.[34,35] There is no chemical reaction either between the reactants and Au nanoparticles, or between the reactants and the polymers. In all experiments, we worked at a basic pH (the initial solution pH = 10.50), to minimize the decomposition of BH_4^-,[44] and at a BH_4^- concentration (2.5×10^{-4} M) in large excess with respect to $Fe(CN)_6^{3-}$ (5.0×10^{-6} M). In this section, the rate of this reaction was monitored by using the conventional spectroscopic method through following the decrease of the $Fe(CN)_6^{3-}$ absorption (A_t at the reaction time t) at 420 nm, and the conversion was given directly by the ratio of $(A_t - A_\infty)/(A_0 - A_\infty)$.

In a control experiment in the absence of the Au@p(NIPAM-Am) hybrid microgels, the non-catalyzed reaction pathway can be neglected, because it is very slow with a half-life of ≥83 min at a solution temperature of $T = 25.0$ °C, in accordance with that reported in the literature.[34] When the hybrid microgels were added, the reaction dramatically increased. For instance, with a Au concentration of 1.8×10^{15} Au-atom mL^{-1}, the half-life was shortened to *ca.* 9 min (Fig. 6a) under the same conditions (pH = 10.50, $T = 25.0$ °C, and an inert atmosphere) and the same starting reactant concentrations. Interestingly, from the spectra shown in Fig. 6a, it can be clearly observed that the LSPR band of the Au nanoparticle cores markedly changed as the catalyzed reduction of $Fe(CN)_6^{3-}$ proceeded. When the hybrid microgels were carefully separated and purified, the LSPR band readily returned to nearly the same profile as that of the as-prepared ones (Fig. 6b; the slight drop in intensity is possibly due to a loss of the hybrid microgels during recycling), proving that the immediate physicochemical microenvironment of the Au nanoparticle cores of the hybrid microgels changed during the catalysis (this confirms the *in situ* LSPR monitoring of the catalyzed chemical reaction, as shown in the next section in detail), meanwhile the Au nanoparticle cores remained stable and no aggregation took place.

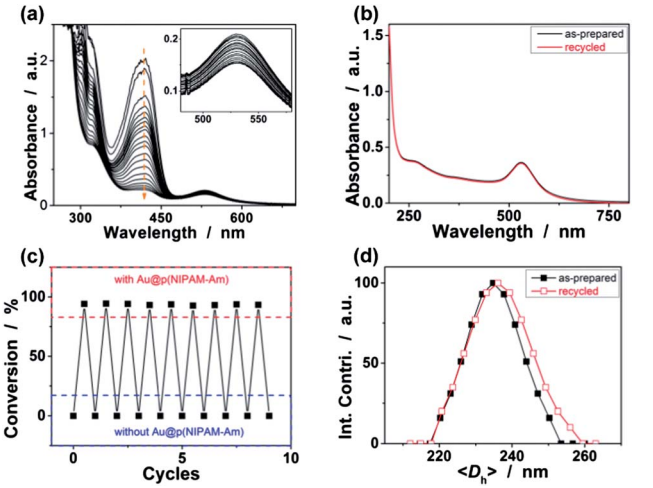

Fig. 6 (a) Time-domain UV-vis spectra of the reaction mixture during the reduction of $Fe(CN)_6^{3-}$ ions catalyzed by Au@p(NIPAM-Am) hybrid microgels. (b) UV-vis spectra of the hybrid microgels before and after use, where the recycled hybrid microgels were separated by centrifugation, purified by dialysis, and redispersed into solution. (c) A comparison of catalysis activity during nine cycles of use, where the conversion was measured after reacting for 150 min. (d) DLS size distribution of the hybrid microgels before and after nine cycles of use. All measurements were made at 25.0 °C.

In order to check the reusability of the Au@p(NIPAM-Am) hybrid microgels, the reduction of $Fe(CN)_6^{3-}$ was repeated nine times with the same hybrid microgels, through sequential addition of the recycled hybrid microgels to a series of aqueous solutions containing a constant concentration of both $Fe(CN)_6^{3-}$ (5.0×10^{-6} M) and BH_4^- (2.5×10^{-4} M) at 25.0 °C and pH = 10.50. The experiments showed that the recycled hybrid microgels exhibited a catalytic activity similar to the as-prepared ones. A high degree (>83%) of reduction of $Fe(CN)_6^{3-}$ can be achieved in 60 min, and complete reduction can be achieved within 150 min, even after nine cycles of use of the hybrid microgels (Fig. 6c). Moreover, Fig. 6d shows the DLS size distribution of the hybrid microgels before and after nine cycles of use; clearly, the size of the hybrid microgels remains largely unchanged. Therefore, these results provide direct proof for their reusability in catalysis, as well as additional confirmation of the stability of the hybrid microgels in the reaction medium.

It is known that Au nanoparticles can change the order of a reaction with respect to the reactants. While the direct reduction of $Fe(CN)_6^{3-}$ with BH_4^- ions has been reported to follow zero-order kinetics with respect to the concentration of $Fe(CN)_6^{3-}$, when Au nanoparticles were present, pseudo-first-

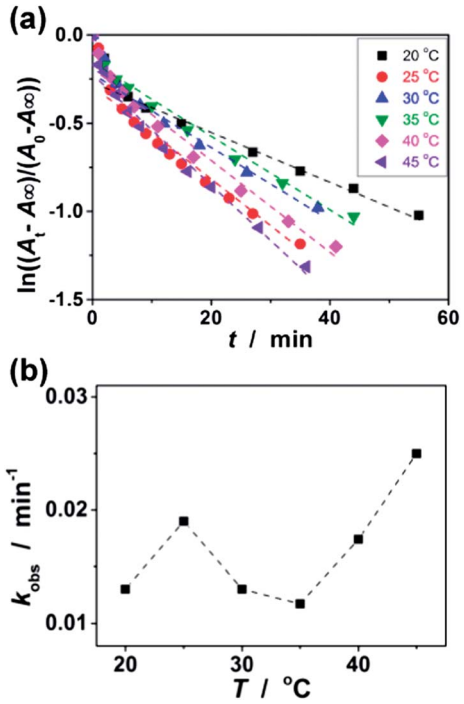

Fig. 7 (a) Typical time trace of the absorption of $Fe(CN)_6^{3-}$ ions at 420 nm during their reduction. (b) A k_{obs}–T plot showing the temperature-modulated catalysis activity.

order kinetics have consistently been observed.[34,35] Fig. 7a shows that this is the case for the solution temperature ranging from 20.0 to 45.0 °C. Linear relationships between $\ln((A_t - A_\infty)/(A_0 - A_\infty))$ and t are obtained in all cases at proper conversions. Deviations from linearity are only seen for very low (<10%) or high degrees of conversion (>75%). However, for the present purpose it suffices to discuss the reaction rates. The rate constant k_{obs} can be accurately determined from the line section.[35]

The rate constants k_{obs} obtained from the $\ln((A_t - A_\infty)/(A_0 - A_\infty)) - t$ plots are shown in Fig. 7b. It is noted that k_{obs} does not exhibit typical dependence on the solution temperature. Instead of a simple linear relationship between k_{obs} and T, the change in k_{obs} with solution temperature can be divided into three regions: at solution temperatures of $T \leq$ *ca.* 25 °C, k_{obs} increases with temperature, whereas in the region of *ca.* 25–33 °C k_{obs} decreases with increasing temperature, and at $T \geq$ *ca.* 35 °C k_{obs} increases again. Clearly, the catalytic activity of the Au nanoparticle cores can be modulated by temperature in a non-monotonous way over a wide range. As indicated above, the modulation of the catalytic activity can be explained on the basis of the temperature-responsive volume phase transition of the hybrid microgels.[4–11] At low temperatures, the polymer gel shell is in the fully swollen state; the reactants can easily diffuse through the pores and reach the Au nanoparticle core surface, so that k_{obs} increases with temperature, as expected from Arrhenius' law.[4,10] In the vicinity of the transition region, the $\langle D_h \rangle$ starts to decrease (the polymer gel shell shrinks), which leads to the expulsion of water and compression of the porous network. This decrease in porosity affects the diffusion of reactants through the polymer gel shell, which slows down as the temperature is increased, thus leading to a decrease in k_{obs}. The results indicate that this decrease in the diffusion coefficients is not compensated by the Arrhenius-like increase in reaction rate with temperature. Once the polymer gel shell is collapsed to some extent, the diffusion of reactants is only slightly or even no longer affected by changes in the polymer gel shell. If the solution temperature increases further, the strong increase in reaction rate with temperature dominates and k_{obs} rises again.

Label-free *in situ* LSPR monitoring of the chemical reaction

Having demonstrated the modulation of the catalysis of the Au@p(NIPAM-Am) hybrid microgels, we next investigated the feasibility of label-free *in situ* LSPR monitoring of the model reaction, *i.e.*, the Au-catalyzed reduction of $Fe(CN)_6^{3-}$ (5.0×10^{-6} M) by BH_4^- ions (2.5×10^{-4} M) in water, at pH = 10.50, and in an inert atmosphere. As mentioned above, the LSPR band of the Au nanoparticle cores markedly changed as the catalyzed reduction of $Fe(CN)_6^{3-}$ proceeded at 25.0 °C (Fig. 6a). The variation in the LSPR intensity (I_t at reaction time t) of the hybrid microgels is summarized in Fig. 8a, from which two stages can be observed: (i) at low conversions (<75%), the LSPR intensity decreased as the reaction proceeded and then gradually plateaued; (ii) as the reaction proceeded further (at high degrees of conversion, *i.e.*, >86%), the LSPR intensity increased until reaching a certain value which was lower than the original one. With the curve in Fig. 5b serving as a calibration, the

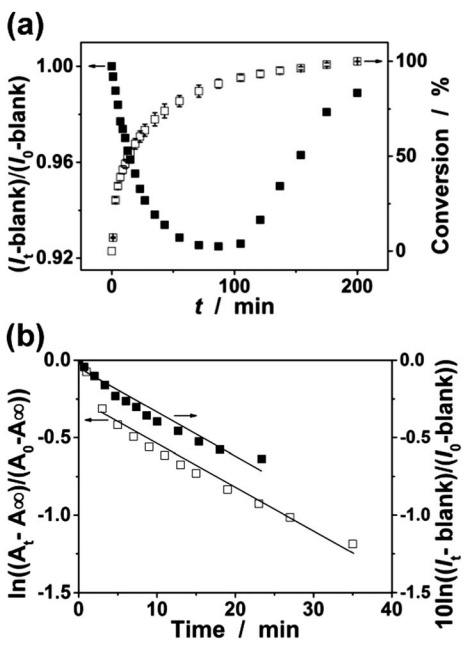

Fig. 8 (a) Time trace of the LSPR intensity of the Au@p(NIPAM-Am) hybrid microgels, and (b) kinetic trace of LSPR during the catalyzed reduction of $Fe(CN)_6^{3-}$ ions. The time-domain conversion and kinetic curve measured with the $Fe(CN)_6^{3-}$ absorption (open symbols) are presented for comparison. All measurements were made at 25.0 °C.

apparent pH value around the Au nanoparticle core could be obtained from the LSPR reading, from which it was estimated that the pH value may decrease to as low as around 9.3 (Fig. S2 in ESI†). Changes in the LSPR intensity at low conversions of the catalyzed chemical reaction correlated well with pseudo-first-order kinetics (Fig. 8b), and mirrored those monitored by using the conventional spectroscopic method through following the decrease of the $Fe(CN)_6^{3-}$ absorption also at low conversions. The catalyzed chemical reaction measured with *in situ* LSPR exhibited a similar apparent rate constant k_{LSPR} of 2.0×10^{-2} min^{-1} to that measured with the $Fe(CN)_6^{3-}$ absorption ($k_{obs} = 1.9 \times 10^{-2}$ min^{-1}) under otherwise the same reaction conditions. These results suggest that the hybrid microgels should allow label-free *in situ* LSPR monitoring of the catalyzed chemical reaction.

There are two main ways, among others, to better understand the label-free *in situ* LSPR response of the Au@p(NIPAM-Am) hybrid microgels. One relates to changes in the shape, size, or even composition of the Au nanoparticle cores. However, this can be excluded by the fact that the LSPR band can be readily recovered when the hybrid microgels are purified after participating in the catalyzed chemical reaction (Fig. 6b), which is clear evidence that the Au nanoparticle cores are stable. This can be further confirmed by the result of a control experiment, when Au@p(NIPAM-Am) hybrid microgels were replaced with Au nanoparticles under otherwise the same conditions. From the spectra shown in Fig. 9a, it can be clearly observed that, during the period required for significant weakening of the $Fe(CN)_6^{3-}$ absorption band (until $(A_t - A_\infty)/(A_0 - A_\infty) < 0.10$, *i.e.*, at high degrees of conversion), the LSPR band of the Au nanoparticles remained totally unchanged. We speculate that the label-free *in situ* LSPR response of the Au@p(NIPAM-Am) hybrid microgels is associated with the changes in local refractive index of the polymer gel shell at the surface of the Au nanoparticle cores during the pH-responsive volume phase transitions, which should provide the second and substantial scenario. In principle, the H^+ ions produced from the Au-catalyzed reduction of $Fe(CN)_6^{3-}$ ions would lead to a decrease in the local pH value, and thus induce conformational changes in the polymer gel network chains at the surface of the Au nanoparticle cores. Large conformational changes in the polymer gel network chains may exhibit as a volume phase transition of the polymer gels (Fig. S3 in ESI†),[22–25] which can result in an LSPR response as has been demonstrated above (Fig. 5). The hypothesis can be supported by another control experiment, where Au@p(NIPAM-Am) hybrid microgels were replaced with pH-insensitive Au@p(NIPAM) hybrid microgels under otherwise the same conditions, and no significant change in the LSPR band was observed during the catalyzed chemical reaction (Fig. 9b), in accordance with that reported previously.[10] In addition, changes in the concentration of hexacyanoferrate(II), hexacyanoferrate(III), borohydride, or borate ions during the catalyzed chemical reaction have been demonstrated to have a negligible effect on the pH-responsive LSPR of the Au@p(NIPAM-Am) hybrid microgels. Thus, the label-free *in situ* LSPR response of Au@p(NIPAM-Am) hybrid microgels could be useful for providing mechanistic insights into Au-catalyzed chemical reactions.

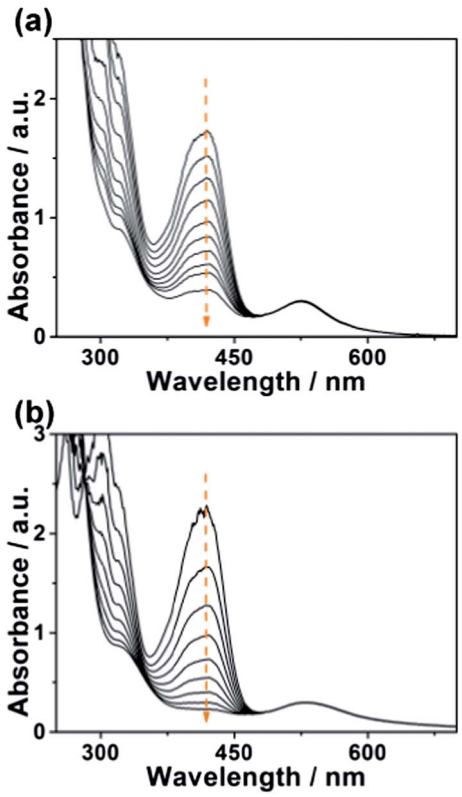

Fig. 9 Time-domain UV-vis spectra of the reaction mixture during the reduction of $Fe(CN)_6^{3-}$ ions catalyzed by (a) Au nanoparticles and (b) Au@p(NIPAM) hybrid microgels. All measurements were made at 25.0 °C.

Fig. 10a shows the effect of the solution temperature on the pseudo-first-order rate constant k_{LSPR} measured by using the label-free *in situ* LSPR response of the Au@p(NIPAM-Am) hybrid microgels. Three different regions can be distinguished in this plot: at temperatures below *ca.* 25 °C, k_{LSPR} increases with temperature, whereas in the region of *ca.* 25–33 °C, k_{LSPR} decreases with increasing temperature, and at temperatures above *ca.* 35 °C k_{LSPR} increases again. In comparison with the k_{obs}–T plot (Fig. 7b), k_{LSPR} revealed nearly the same trend towards temperature change (Fig. 10a), clearly correlating the kinetics measured by the label-free *in situ* LSPR response to those measured by the conventional spectroscopic method utilizing the $Fe(CN)_6^{3-}$ absorption. Therefore, these results can not only provide a further confirmation of the feasibility of the hybrid microgels for label-free *in situ* LSPR monitoring of the catalyzed chemical reaction, but also indicate that the kinetics measured by both methods revealed nearly the same trend at the investigated temperatures.

Since both k_{LSPR} and k_{obs} exhibit a conventional Arrhenius-type dependence on the solution temperature at the regimes of $T \leq$ *ca.* 25 °C (corresponding to the swollen state of the polymer gel shell) and $T \geq$ *ca.* 35 °C (collapsed state),[10,34,35] respectively, the apparent activation energy (E_a) and the pre-exponential factor (A) can be determined on the basis of the linear fitting of

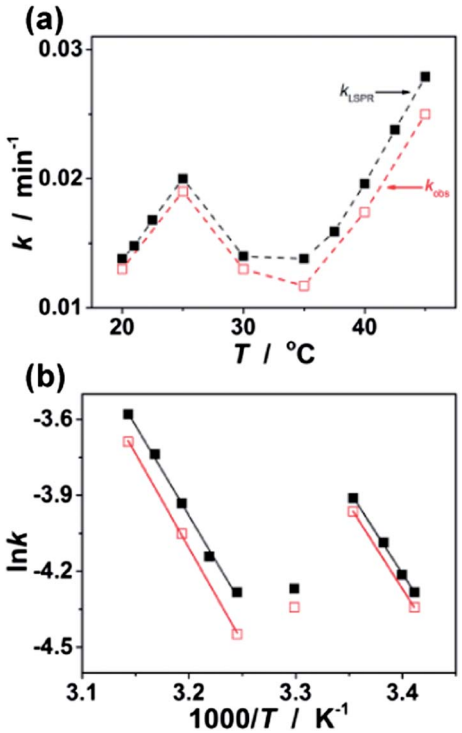

Fig. 10 (a) The k–T and (b) $\ln k$ – $1000/T^{-1}$ plots showing the temperature-modulated catalysis, measured with the $Fe(CN)_6^{3-}$ absorption (□; $k = k_{obs}$) and the LSPR (■; $k = k_{LSPR}$), respectively. The solid lines shown in (b) are linear fits of the plots at each temperature regime.

$\ln k$ (here k is k_{LSPR} or k_{obs}) *versus* T^{-1} (Fig. 10b) and the Arrhenius equation:[45]

$$\ln k = \ln A - E_a/RT \quad (4)$$

The apparent activation parameters are summarized in Table 1. While the interpretation of the apparent activation parameters is complicated by the fact that these represent the combination of the diffusion and catalysis processes,[10] for the results measured with either the label-free *in situ* LSPR or the conventional spectroscopic method, the observation that the E_a increased when temperature increased above *ca.* 35 °C may be consistent with a model where diffusion is rate-limiting;[10] the collapsed polymer gel shell could be envisaged to require more energy for the reactant to move. More importantly, in comparison with the apparent activation parameters measured with the $Fe(CN)_6^{3-}$ absorption, the smaller A values (indicating a smaller total number of collisions per minute),[45] as well as the smaller E_a values (indicating a lower energy required to reach the transition state of the reactants, thereby a lower energy required to initiate the chemical reaction),[45] were obtained by the label-free *in situ* LSPR monitoring. The observed difference between the thermodynamics measured by the two methods could be reasonable when considering that different from the conventional spectroscopic method which only reflects the overall information occurring in the reaction system, the label-free *in situ* LSPR monitoring gives local information occurring on the catalytic surface and in a relatively confined volume. Therefore, the label-free *in situ* LSPR monitoring has the potential to advance our understanding of the catalyzed chemical reaction under realistic conditions.

Table 1 The apparent activation parameters for the catalyzed reduction of $Fe(CN)_6^{3-}$

	Measured with *in situ* LSPR		Measured with $Fe(CN)_6^{3-}$ absorption	
Temperature range (°C)	A (min^{-1})	E_a (kJ mol^{-1})	A (min^{-1})	E_a (kJ mol^{-1})
≤25	6.9×10^7	54.4	8.7×10^7	55.2
≥35	1.4×10^8	59.0	3.7×10^8	61.9

Conclusion

We developed a class of metal@polymer hybrid microgels comprising of Au nanoparticles covered with a temperature and pH dual-responsive copolymer gel shell of p(NIPAM-Am), with which we further demonstrated the feasibility that a metal@polymer hybrid microgel under a rational design can not only allow modulation of the catalytic activity of the noble metal nanoparticle cores, but also allow label-free *in situ* LSPR monitoring of the catalyzed chemical reaction. While the catalytic activity can be tuned through varying the solution temperature, the kinetics and thermodynamics of the catalyzed chemical reaction can be measured by label-free *in situ* LSPR monitoring. Unlike the conventional spectroscopic methods that only reflect the overall information occurring in the reaction system, label-free *in situ* LSPR monitoring gives local information occurring on the catalytic surface and therefore has the potential to advance our understanding of the catalyzed chemical reaction. Although in the presented case the *in situ* LSPR monitoring is currently limited to the response to local pH, with the significant advances that have been achieved in the design of polymer gels that can respond to specific molecular species, we anticipate that this study may serve as a starting point for the development of smart reactors/catalysts for the simultaneous modulation and monitoring of the catalyzed chemical reaction, which should significantly expand the range of their applications.

Acknowledgements

We gratefully acknowledge the financial support from the National Science Foundation of China (21274118, 91227120, and 20923004), the Program for New Century Excellent Talents in University of Ministry of Education of China (NCET-13-0506), the Natural Science Foundation for Distinguished Young Scholars of Fujian Province, the Program for New Century Excellent Talents in Fujian Province University, the Fundamental Research Funds for the Central Universities (2012121016), and the National Fund for Fostering Talents of Basic Science (J1310024).

References

1 J. Zhang, S. Xu and E. Kumacheva, *J. Am. Chem. Soc.*, 2004, **126**, 7908.
2 D. Suzuki and H. Kawaguchi, *Langmuir*, 2006, **22**, 3818.
3 J. H. Kim and T. R. Lee, *Langmuir*, 2007, **23**, 6504.
4 Y. Lu, Y. Mei, M. Drechsler and M. Ballauff, *Angew. Chem., Int. Ed.*, 2006, **45**, 813.
5 Y. Lu, S. Proch, M. Schrinner, M. Drechsler, R. Kempe and M. Ballauff, *J. Mater. Chem.*, 2009, **19**, 3955.
6 Y. Lu, J. Yuan, F. Polzer, M. Drechsler and J. Preussner, *ACS Nano*, 2010, **4**, 7078.
7 N. Welsch, M. Ballauff and Y. Lu, *Adv. Polym. Sci.*, 2010, **234**, 129.
8 Y. Lu and M. Ballauff, *Prog. Polym. Sci.*, 2011, **36**, 767.
9 R. Contreras-Cáceres, A. Sánchez-Iglesias, M. Karg, I. Pastoriza-Santos, J. Pérez-Juste, J. Pacifico, T. Hellweg, A. Fernández-Barbero and L. M. Liz-Marzán, *Adv. Mater.*, 2008, **20**, 1666.
10 S. Carregal-Romero, N. J. Buurma, J. Pérez-Juste, L. M. Liz-Marzán and P. Hervés, *Chem. Mater.*, 2010, **22**, 3051.
11 J. Pérez-Juste, I. Pastoriza-Santos and L. M. Liz-Marzán, *J. Mater. Chem. A*, 2013, **1**, 20.
12 C. F. Xiao, S. M. Chen, L. Y. Zhang, S. Q. Zhou and W. T. Wu, *Chem. Commun.*, 2012, **48**, 11751.
13 W. T. Wu, N. Mitra, E. C. Y. Yan and S. Q. Zhou, *ACS Nano*, 2010, **4**, 4831.
14 Y. D. Yin, R. M. Rioux, C. K. Erdonmez, S. Hughes, G. A. Somorjai and A. P. Alivisatos, *Science*, 2004, **304**, 711.
15 X. Q. Huang, C. Y. Guo, J. Q. Zou, N. F. Zheng and G. D. Stucky, *Small*, 2009, **5**, 361.
16 N. J. Halas, *Nano Lett.*, 2010, **10**, 3816.
17 K. D. Osberg, M. Rycenga, N. Harris, A. L. Schmucker, M. R. Langille, G. C. Schatz and C. A. Mirkin, *Nano Lett.*, 2012, **12**, 3828.
18 J. Zeng, Q. Zhang, J. Y. Chen and Y. N. Xia, *Nano Lett.*, 2010, **10**, 30.
19 X. Xia, S. Xie, M. Liu, H. Peng, N. Lu, J. Wang, M. J. Kim and Y. N. Xia, *Proc. Natl. Acad. Sci. U. S. A.*, 2013, **110**, 6669.
20 L. Yang, S. Shan, R. Loukrakpam, V. Petkov, Y. Ren, B. Wanjala, M. Engelhard, J. Luo, J. Yin, Y. Chen and C. J. Zhong, *J. Am. Chem. Soc.*, 2012, **134**, 15048.
21 S. Shan, V. Petkov, L. Yang, D. Mott, B. N. Wanjala, F. Cai, B. H. Chen, J. Luo and C. J. Zhong, *ACS Catal.*, 2013, **3**, 3075.
22 C. Wu and S. Q. Zhou, *Macromolecules*, 1997, **30**, 574.
23 B. H. Tan and K. C. Tam, *Adv. Colloid Interface Sci.*, 2008, **136**, 25.
24 L. A. Lyon, Z. Meng, N. Singh, C. D. Sorrell and A. S. John, *Chem. Soc. Rev.*, 2009, **38**, 865.
25 T. Ye, S. Yan, Y. Hu, L. Ding and W. T. Wu, *Polym. Chem.*, 2014, **5**, 186.
26 X. He, M. Aizenberg, O. Kuksenok, L. D. Zarzar, A. Shastri, A. C. Balazs and J. Aizenberg, *Nature*, 2012, **487**, 214.
27 F. Hapiot, S. Menuel and E. Monflier, *ACS Catal.*, 2013, **3**, 1006.
28 P. Mulvaney, *Langmuir*, 1996, **12**, 788.
29 B. Chowdhury, J. J. Bravo-Suárez, N. Mimura, J. Q. Lu, K. K. Bando, S. Tsubota and M. Haruta, *J. Phys. Chem. B*, 2006, **110**, 22995.
30 J. F. Li, Y. F. Huang, Y. Ding, Z. L. Yang, S. B. Li, X. S. Zhou, F. R. Fan, W. Zhang, Z. Y. Zhou, D. Y. Wu, B. Ren, Z. L. Wang and Z. Q. Tian, *Nature*, 2010, **464**, 392.
31 A. Tittl, X. H. Yin, H. Giessen, X.-D. Tian, Z.-Q. Tian, C. Kremers, D. N. Chigrin and N. Liu, *Nano Lett.*, 2013, **13**, 1816.
32 W. Xie, B. Walkenfort and S. Schlücker, *J. Am. Chem. Soc.*, 2013, **135**, 1657.
33 C. Vázquez-Vázquez, B. Vaz, V. Giannini, M. Pérez-Lorenzo, R. A. Alvarez-Puebla and M. A. Correa-Duarte, *J. Am. Chem. Soc.*, 2013, **135**, 13616.
34 S. Carregal-Romoero, J. Pérez-Juste, P. Hervés, L. M. Liz-Márzan and P. Mulvaney, *Langmuir*, 2010, **26**, 1271.
35 P. Hervés, M. Pérez-Lorenzo, L. M. Liz-Marzán, J. Dzubiella, Y. Lu and M. Ballauff, *Chem. Soc. Rev.*, 2012, **41**, 5577.
36 B. Chu, *Laser Light Scattering*, Academic Press, New York, 2nd edn 1991.
37 S. N. Baker, T. M. McCleskey and G. A. Baker, *Ionic liquids IIIB: fundamentals, progress, challenges and opportunities: transformations and processes* (ACS Symposium Series, no. 902), American Chemical Society, Washington D.C., 2005.
38 T. Hoare and D. McLean, *Macromol. Theory Simul.*, 2006, **15**, 619.
39 Z. Abe, H. Tanaka and M. Sumimoto, *J. Polym. Sci., Polym. Chem. Ed.*, 1978, **16**, 305.
40 D. I. Gittins and F. Caruso, *J. Phys. Chem. B*, 2001, **105**, 6846.
41 K. S. Mayya, B. Schoeler and F. Caruso, *Adv. Funct. Mater.*, 2003, **13**, 183.
42 G. Schneider and G. Decher, *Nano Lett.*, 2004, **4**, 1833.
43 T. J. Freund, *J. Inorg. Nucl. Chem.*, 1959, **9**, 246.
44 M. Bhattacharjee, A. K. Bhattacharjee and M. K. Mahanti, *Bull. Chem. Soc. Jpn.*, 1981, **54**, 3566.
45 K. J. Laidler, *The World of Physical Chemistry*, Oxford University Press, 1993.